Detection prospects of dark matter in the Einstein Telescope

Chuan-Ren Chen* and Chrisna Setyo Nugroho†
Department of Physics, National Taiwan Normal University, Taipei 116, Taiwan

(Received 29 November 2021; accepted 22 March 2022; published 8 April 2022)

We improve the calculations of the elastic motion induced by dark matter hitting the surface of the mirror inside an interferometer used for gravitational-wave detection. We focus on the discovery potential of such a dark matter signal in the third-generation European gravitational-wave detector, the Einstein Telescope. By taking the thickness of the mirror into account, more than one resonance is predicted in the sensitive regime of the high-frequency interferometer. When the mass of dark matter is heavier than a few PeV or is highly boosted, the signal-to-noise ratio could exceed one, and the Einstein Telescope should be able to detect this dark matter signal.

DOI: 10.1103/PhysRevD.105.083001

I. INTRODUCTION

The existence of dark matter (DM) provides explanations for several astronomical observations, such asthe rotational curves of galaxies. However, except for gravitational effects, we know very little about its physical properties, including its spin and mass. In other words, the DM particle could be a boson or a fermion, and its mass could range from below an eV to greater than a TeV. Even though no conclusive evidence of a DM signal has been found in the laboratory, some observations, if interpreted as signals of DM, give us hits about the mass of DM. The recoil energy detection in the XENON1T experiment [1] may imply dark matter with mass of $O(1)$ keV; the excesses of cosmic-ray positrons observed by PAMELA [2] and AMS-02 [3] suggest that the mass of dark matter should be heavier than a few hundred GeV; and the observations of PeV neutrino events by IceCube point to super heavy dark matter.

To claim the discovery of dark matter relies on the detection of the recoil energy of either an electron or nucleus inside a detector caused by dark matter scattering, e.g., the XENON1T experiment. However, interestingly, the technology used in the discovery of gravitational waves (GWs) by LIGO and VIRGO in 2016 [4] provides another method for dark matter detection. The idea for GW detection is that as GWs pass through the Earth, the tidal force causes tiny shifts in the length of the LIGO/VIRGO arms, which can be detected by the laser interferometer. Similarly, when dark matter particles pass through the interferometer and hit the mirror of the interferometer, the recoil of the mirror may generate detectable vibration signals. The geometric properties of the mirror and the mass of the dark matter particle determine the characteristic frequencies. The details of such a scenario have been discussed in Ref. [5]. In this paper, we take into account the thickness of the mirror and the noise caused by the thermal fluctuations, which have been neglected. We consider LIGO/VIRGO, KAGRA, and the proposed Einstein Telescope (ET), and focus on ET since its high-frequency interferometer has a better chance of detecting a signal (as will be shown later). Actually, various approaches to search for DM with GW detectors have been discussed in the literature; see, for instance, Refs. [6–33].

The rest of this paper is organized as follows. In Sec. II we give a detailed derivation of the signal due to the collision of dark matter particles with the mirror. In Sec. III we discuss the noises, with an emphasis on internal thermal noises. We show the signal-to-noise ratio in Sec. IV. Our summary and conclusions are presented in Sec. V.

II. DARK MATTER SIGNAL

We focus on the elastic oscillation of the mirror due to the collisions of DM particles. We assume that the test mass used in the interferometer (TM) collides with a DM particle at $t = 0$. During the collision, the DM transfers a recoil momentum q_R to the TM. Following Refs. [5,6], the external force can be given by

$$F_{\rm DM} = q_R \delta(t). \tag{2.1}$$

This collision induces a transverse deflection $z_{\rm Elas}$ on the surface of the mirror and causes the elastic oscillation of the mirror. For $t > 0$, the corresponding equations of motion of the TM with mass M_T due to this collision are [34,35]

*crchen@ntnu.edu.tw
†setyo13nugros@ntnu.edu.tw

$$\frac{\partial M_r}{\partial r}+\frac{1}{r}\frac{\partial M_{r\theta}}{\partial \theta}+\frac{M_r-M_\theta}{r}-Q_r-\frac{\rho h^3}{12}\frac{\partial^2\psi_r}{\partial t^2}=0,$$
$$\frac{\partial M_{r\theta}}{\partial r}+\frac{1}{r}\frac{\partial M_\theta}{\partial \theta}+\frac{2M_{r\theta}}{r}-Q_\theta-\frac{\rho h^3}{12}\frac{\partial^2\psi_\theta}{\partial t^2}=0,$$
$$\frac{\partial Q_r}{\partial r}+\frac{1}{r}\frac{\partial Q_\theta}{\partial \theta}+\frac{Q_r}{r}-\frac{\rho h\omega_e}{Q_M}\frac{\partial z_{\rm Elas}}{\partial t}-\rho h\frac{\partial^2 z_{\rm Elas}}{\partial t^2}=0, \quad (2.2)$$

with the following initial conditions for $z_{\rm Elas}$:

$$z_{\rm Elas}(r,\theta,t=0)=0,$$
$$\dot{z}_{\rm Elas}(r,\theta,t=0)=\frac{q_R}{M_T}\pi a^2\delta(\vec{r}-\vec{r}_0), \quad (2.3)$$

where $\dot{z}_{\rm Elas}\equiv\frac{\partial z_{\rm Elas}}{\partial t}$. Here h, a, ρ, Q_M, and ω_e denote the thickness, radius, mass density, quality factor, and angular eigenfrequency of the mirror. The vector $\vec{r}_0=(r_0,\theta_0)$ specifies the location where the DM particle collides with the mirror. The components of the mirror moments M_i and shearing forces Q_i can be expressed in terms of the transverse deflection $z_{\rm Elas}$ as well as the angular bending rotation of the normal to the neutral surface in radial and circumferential directions, ψ_r and ψ_θ, as [34]

$$M_r=D\left[\frac{\partial\psi_r}{\partial r}+\frac{\nu}{r}\left(\psi_r+\frac{\partial\psi_\theta}{\partial\theta}\right)\right],$$
$$M_\theta=D\left[\frac{1}{r}\left(\psi_r+\frac{\partial\psi_\theta}{\partial\theta}\right)+\nu\frac{\partial\psi_r}{\partial r}\right],$$
$$M_{r\theta}=\frac{D}{2}(1-\nu)\left[\frac{1}{r}\left(\frac{\partial\psi_r}{\partial\theta}-\psi_\theta\right)+\frac{\partial\psi_\theta}{\partial r}\right],$$
$$Q_r=\kappa^2 Gh\left(\psi_r+\frac{\partial z_{\rm Elas}}{\partial r}\right),$$
$$Q_\theta=\kappa^2 Gh\left(\psi_\theta+\frac{1}{r}\frac{\partial z_{\rm Elas}}{\partial\theta}\right), \quad (2.4)$$

where the flexural rigidity of the mirror D is written in terms of the Young's modulus E and Poisson ratio ν as $D=Eh^3/12(1-\nu^2)$. In Eq. (2.4), G stands for the shear modulus and $\kappa^2=\pi^2/12$ is the shear coefficient. Note that Eq. (2.2) is different from Kirchhoff thin plate theory [36,37] used in Ref. [5].

The general solution of Eq. (2.2) for $z_{\rm Elas}$ can be written as

$$z_{\rm Elas}(r,\theta,r_0,\theta_0,t)=\Theta(t)\frac{1}{\sqrt{1-\frac{1}{4Q_M^2}}}\times\sum_{m,n=0}^{m,n=\infty}K_{mn}(r_0,\theta_0)W_{mn}(r,\theta)\times\exp\left[-\frac{\omega_{mn}}{2Q_M}t\right]\sin\left(\omega_{mn}\sqrt{1-\frac{1}{4Q_M^2}}t\right), \quad (2.5)$$

where m is the number of nodal diameters, n denotes the number of nodal circles, and ω_{mn} corresponds to the eigenfrequencies for each mode. The coefficient $K_{mn}(r_0,\theta_0)$ depends on the location of the DM hit on the mirror.[1] The function $W_{mn}(r,\theta)$ can be obtained by redefining the problem in terms of three potentials w_1, w_2, w_3 as [38]

$$\psi_r=(\sigma_1-1)\frac{\partial w_1}{\partial r}+(\sigma_2-1)\frac{\partial w_2}{\partial r}+\frac{1}{r}\frac{\partial w_3}{\partial\theta},$$
$$\psi_\theta=(\sigma_1-1)\frac{1}{r}\frac{\partial w_1}{\partial\theta}+(\sigma_2-1)\frac{1}{r}\frac{\partial w_2}{\partial\theta}-\frac{\partial w_3}{\partial r},$$
$$W=w_1+w_2, \quad (2.6)$$

where we have suppressed the m and n indices. These potentials w_i satisfy the following equations in polar coordinates:

$$(\nabla^2+\delta_i^2)w_i=0, \quad (2.7)$$

where i runs from 1 to 3 and the Laplacian operator $\nabla^2=\partial^2/\partial\chi^2+(1/\chi)\partial/\partial\chi+(1/\chi)^2\partial^2/\partial\theta^2$ is expressed in terms of the dimensionless quantity $\chi=r/a$. In Eqs. (2.6) and (2.7) we introduced the dimensionless parameters

$$\delta_1^2,\delta_2^2=\frac{1}{2}\lambda^2\{R+S\pm[(R-S)^2+4\lambda^{-2}]^{1/2}\},$$
$$\delta_3^2=\frac{2}{(1-\nu)}(R\lambda^2-S^{-1}),$$
$$\sigma_1,\sigma_2=(\delta_2^2,\delta_1^2)(R\lambda^2-S^{-1})^{-1},$$
$$R=(h/a)^2/12,$$
$$S=D/(\kappa^2Ga^2h)=[2/(\pi^2(1-\nu))](h/a)^2. \quad (2.8)$$

These parameters are functions of the dimensionless frequency parameter λ (or, more accurately, λ_{mn}),

$$\lambda_{mn}=\omega_{mn}a^2\left(\frac{\rho h}{D}\right)^{1/2}, \quad (2.9)$$

[1]This implies that the transverse deflection of the mirror $z_{\rm Elas}$ becomes r_0 and θ_0 dependent, as explicitly written in Eq. (2.5).

TABLE I. Properties of the mirrors used in the interferometers for different GW experiments [5,40].

	LIGO, VIRGO	KAGRA	LF-ET	HF-ET
Material	Fused silica	Sapphire	Silicon	Fused silica
Mirror mass M_T (kg)	40	22.8	211	200
Thickness h (cm)	20	15	50	30
Radius a (cm)	17.5	11	22.5	31
Mass density ρ (g/cm^3)	2.20	4.00	2.33	2.20
Young's modulus E (GPa)	72	400	188	72
Poisson ratio ν	0.17	0.30	0.22	0.17

where we have restored the m and n indices. The general solutions of Eq. (2.7) are given in terms of the product of the radial and angular functions as

$$\begin{aligned} w_1 &= A_1 R_m(\Delta_1(\lambda_{mn})\chi)\cos(m\theta), \\ w_2 &= A_2 R_m(\Delta_2(\lambda_{mn})\chi)\cos(m\theta), \\ w_3 &= A_3 R_m(\Delta_3(\lambda_{mn})\chi)\sin(m\theta), \end{aligned} \tag{2.10}$$

where Δ_i is a function of λ_{mn}. Furthermore, it also depends on the sign of δ_i^2 as [39]

$$\Delta_i = \{\, \delta_i \quad \text{if } \delta_i^2 \geq 0\,, \tag{2.11a}$$

$$\Delta_i = \{\, \mathrm{Im}(\delta_i) \quad \text{if } \delta_i^2 < 0\,, \tag{2.11b}$$

The function R_m is given in terms of the Bessel function of the first kind J_m and its modified version I_m as

$$R_m(\Delta_i\chi) = \{\, J_m(\Delta_i\chi) \quad \text{if } \delta_i^2 \geq 0\,, \tag{2.12a}$$

$$R_m(\Delta_i\chi) = \{\, I_m(\Delta_i\chi) \quad \text{if } \delta_i^2 < 0\,. \tag{2.12b}$$

The frequency parameter λ_{mn} is obtained by assuming that the edges of the mirror used in GW detectors are free. This sets the boundary conditions at $r = a$ as

$$M_r|_{r=a} = M_{r\theta}|_{r=a} = Q_r|_{r=a} = 0. \tag{2.13}$$

Substituting Eqs. (2.4)–(2.6) into the boundary conditions in Eq. (2.13), we arrive at the following matrix equation:

$$\begin{pmatrix} C_{11} & C_{12} & C_{13} \\ C_{21} & C_{22} & C_{23} \\ C_{31} & C_{32} & C_{33} \end{pmatrix} \begin{pmatrix} A_1 \\ A_2 \\ A_3 \end{pmatrix} = \begin{pmatrix} 0 \\ 0 \\ 0 \end{pmatrix}. \tag{2.14}$$

This can be written in vector notation, $\mathbf{C}\vec{A} = \vec{0}$. The elements of the $\mathbf{C}$ matrix are

$$\begin{aligned} C_{1j} &= (\sigma_j - 1)[R_m''(\Delta_j) + \nu R_m'(\Delta_j) - \nu m^2 R_m(\Delta_j)], \\ C_{13} &= m(1-\nu)[R_m'(\Delta_3) - R_m(\Delta_3)], \\ C_{2j} &= -2m(\sigma_j - 1)[R_m'(\Delta_j) - R_m(\Delta_j)], \\ C_{23} &= -[R_m''(\Delta_3) - R_m'(\Delta_3) + m^2 R_m(\Delta_3)], \\ C_{3j} &= \sigma_j R_m'(\Delta_j), \\ C_{33} &= m R_m(\Delta_3), \end{aligned} \tag{2.15}$$

where $R_m'(\Delta_i\chi) = \frac{\partial R_m(\Delta_i\chi)}{\partial\chi}$ and the index j runs from 1 to 2. The nontrivial solution of Eq. (2.14) requires the determinant of the matrix $\mathbf{C}$ to vanish, which further sets the values of the eigenfrequencies.

The properties of the mirrors in both existing and proposed third-generation GW experiments are summarized in Table I. For LIGO, VIRGO, KAGRA, and the low-frequency Einstein Telescope (LF-ET) the lowest eigenfrequencies are 10.74, 10.74, 15.33, and 15.75 kHz, respectively. These frequencies lie outside of their detection bands. This can be understood from Eq. (2.9) and Table I, where the values of the eigenfrequencies are proportional to the ratio of the thickness to the radius h/a, the Young's modulus E, and the mass density of the mirror ρ. On the other hand, the eigenfrequencies of the mirror of the high-frequency Einstein Telescope (HF-ET) are located inside the detection band, as shown in Table II. The quality factor for the HF-ET mirror is 2.5×10^9 [40].[2] We find that there are four resonance peaks inside the HF-ET detection band. This is different from the study of Ref. [5] which found one resonance peak at 7.24 kHz. Furthermore, the thin mirror proposed in Ref. [5] could generate more resonance peaks inside the ET detection band. However (as will be shown below), this is not a suitable option since the resonance peaks are also excited by internal thermal noise of the mirror, causing the detector to lose its sensitivity. From here on, we focus on

[2]We take the loss angle of fused silica provided in Ref. [40]. To keep the validity of the limits set by our subsequent calculation, one must improve the loss angle of the fused silica mirror to overcome the parametric instabilities in the GW detector, as shown in Refs. [41,42].

TABLE II. Numerical values of the eigenfrequencies ($\frac{\omega_{mn}}{2\pi}$) of the HF-ET for the first few values of m and n in units of $\times 10^4$ Hz.

	$m=0$	$m=1$	$m=2$	$m=3$
$n=0$	…	…	0.240	0.485
$n=1$	0.514	0.601	0.791	0.897
$n=2$	0.548	0.635	1.100	1.338
$n=3$	0.643	0.820	1.271	1.455

studying the elastic oscillations of the mirror in the HF-ET induced by DM collisions.

The function $W_{mn}(r,\theta)$ can be determined by expressing the coefficients A_2 and A_3 in terms of A_1 via Eq. (2.14) and using Eq. (2.6) as

$$W_{mn}(r,\theta) = A_1\left[R_m\left(\frac{\Delta_1(\lambda_{mn})}{a}r\right) - \left[\frac{C_{31}C_{23}-C_{21}C_{33}}{C_{32}C_{23}-C_{22}C_{33}}\right] \times R_m\left(\frac{\Delta_2(\lambda_{mn})}{a}r\right)\right]\cos(m\theta). \tag{2.16}$$

The transverse deflection of the mirror $z_{\rm Elas}(r,\theta,t)$ can be determined by inserting Eq. (2.16) back into Eq. (2.5), with the redefinition $A_1 K_{mn} \to K_{mn}$. In GW experiments, the signal of the gravitational waves as well as the noises present in the interferometer are analyzed in terms of the strain amplitude in the frequency domain. Therefore, one needs to do the Fourier transform

$$\tilde{z}_{\rm Elas}(r,\theta,r_0,\theta_0,f) = \int_{-\infty}^{\infty} z_{\rm Elas}(r,\theta,r_0,\theta_0,t)e^{-i2\pi f t}dt \tag{2.17}$$

of the DM signal and evaluate its absolute value in order to write the corresponding strain amplitude of the signal,

$$|\tilde{z}_{\rm Elas}(r,\theta,r_0,\theta_0,f)| = \frac{1}{2\pi}\sum_{m=0}^{m=\infty}\sum_{n=0}^{n=\infty} K_{mn}(r_0,\theta_0)W_{mn}(r,\theta) \times \frac{f_{mn}}{\sqrt{(-f^2+f_{mn}^2)^2+(\frac{f f_{mn}}{Q_M})^2}}, \tag{2.18}$$

where $f_{mn} \equiv \frac{\omega_{mn}}{2\pi}$ is the eigenfrequency of the mirror expressed in hertz. We see that at a resonance frequency $f = f_{mn}$, the elastic oscillation induced by DM collisions has pronounced peaks.

To determine the coefficient K_{mn}, we employ the momentum conservation [5]

$$q_R\delta(\vec{r}-\vec{r}_0) = 2\pi\rho h\sum_{m=0}^{m=\infty}\sum_{n=0}^{n=\infty} K_{mn}W_{mn}(r,\theta)f_{mn}, \tag{2.19}$$

where $\vec{r}_0$ specifies the location of the DM hit on the mirror. We multiply both sides of Eq. (2.19) by $W_{kl}(r,\theta)$ and further integrate over the mirror surface,

$$q_R W_{kl}(r_0,\theta_0) = 2\pi\rho h K_{kl} f_{kl}\int_0^{2\pi}\int_0^a W_{kl}^2(r,\theta)rdrd\theta,$$
$$K_{mn}(r_0,\theta_0) = \frac{q_R W_{mn}(r_0,\theta_0)}{2\pi\rho h f_{mn}\int_0^{2\pi}\int_0^a W_{mn}^2(r,\theta)rdrd\theta}, \tag{2.20}$$

where we changed the indices k, l back to m, n in the last line. The laser beam used in a typical GW detector is focused at the center of the mirror to monitor the differential change of the interferometer arm. Therefore, we evaluate the elastic oscillation at the center of the mirror, which corresponds to the $m=0$ mode or the axis-symmetric mode. In this case, the coefficient K_{mn} reads

$$K_{0n}(r_0,\theta_0) = \frac{q_R W_{0n}(r_0,\theta_0)}{4\pi^2\rho h f_{0n}\int_0^a W_{0n}^2(r)rdr}. \tag{2.21}$$

The magnitudes of $|\tilde{z}_{\rm Elas}|$ at resonance frequencies $f = f_{0n}$ evaluated at $r=0$ for different nodal circle modes n and various collision points on the mirror r_0 are collected in Table III. As can be seen from this table, for each n mode, the highest transverse displacement is reached when DM hits the center of the mirror ($r_0 = 0$). To compare the DM signal with the ET's sensitivity, we need to calculate the strain amplitude induced by DM collisions. It is given by

$$\tilde{h}_{\rm DM}(r,\theta,r_0,\theta_0,f) = \sqrt{\frac{4f}{L^2}}|\tilde{z}_{\rm Elas}(r,\theta,r_0,\theta_0,f)|, \tag{2.22}$$

where L denotes the arm length of the interferometer. We are aware that the resonance modes discussed here can also be excited by the noise. We discuss the relevant noise that may overcome the DM signal in the next section.

III. RELEVANT NOISE

In this section we briefly discuss the noise that affects the sensitivity of ET. The details of the noise components can be found in Ref. [40] and references therein, and therefore we will not repeat them here. We only highlight the dominant noise component that could potentially suppress the DM signal under consideration.

The Einstein Telescope employs a new strategy called the xylophone technique in its design. It combines two interferometers operating in different frequency regimes. One interferometer (LF-ET) is cooled down to cryogenic temperatures at 10 K with a low-power laser to reduce radiation pressure noise. This is designed to have a high sensitivity in the low-frequency regime. On the other hand, the second interferometer (HF-ET) works at room temperature (290 K), and a high-power laser is utilized to reduce the shot noise. This is done to reach a high sensitivity at high frequencies.

TABLE III. Values of $|\tilde{z}_{\rm Elas}(r=0,\theta=0,r_0,\theta_0,f=f_{0n})|\times 10^{-23}$ at different collision points r_0 for $q_R \approx m_{\rm DM} v = 1\ {\rm GeV/c^2} \times 220\ {\rm km/s}$ in units of $\rm cm\,Hz^{-1}$. The resonance frequency for each mode is shown in the second column.

	f_{0n} (kHz)	$r_0 = 0.0\ a$	$r_0 = 0.1\ a$	$r_0 = 0.2\ a$	$r_0 = 0.3\ a$	$r_0 = 0.4\ a$	$r_0 = 0.5\ a$
$n=1$	5.136	282.8	265.1	216.8	150.9	84.67	33.03
$n=2$	5.482	253.6	236.2	189.4	127.0	66.41	22.21
$n=3$	6.431	192.1	175.4	131.9	77.62	31.08	4.828
$n=4$	9.072	163.3	139.8	84.52	30.16	2.431	3.068

As a result, this technique allows ET to gain good sensitivities for both low and high frequencies.

At low frequencies below 10 Hz, the dominant noise components are seismic noise and gravity-gradient noise. In the intermediate regime up to 500 Hz, the relevant noises are suspension thermal noise and internal thermal noise (mirror thermal noise). The internal thermal noise excites the eigenfrequencies of the mirror and may potentially hide the DM signal. In fact, the internal thermal noise of the mirror with the power spectral density (PSD) given by [43]

$$x_{\rm th}^2(f) = \frac{8k_B T}{(2\pi)^3}\sum_{m,n=0}^{m,n=\infty}\frac{\phi_{mn}(f) f_{mn}^2}{M_T f[(f^2-f_{mn}^2)^2+\phi_{mn}^2(f) f_{mn}^4]} \tag{3.1}$$

mimics the DM signal at $f = f_{mn}$. Here, k_B, T, and M_T stand for the Boltzmann constant, temperature, and mirror mass, respectively. In many materials, the mechanical loss angle ϕ_{mn} is approximately a constant over a wide band of frequencies. It characterizes the internal damping of the mirror and is inversely proportional to the quality factor of the mirror, namely, $\phi_{mn} \propto 1/Q_M$. Note that when the temperature drops to zero or the loss angle vanishes, there would be no internal thermal noise, as it should be. The corresponding strain amplitude due to this noise is

$$\tilde{h}_{\rm th}(f) = \sqrt{\frac{4x_{\rm th}^2(f)}{L^2}}. \tag{3.2}$$

On the other hand, the most dominant noise component in the high-frequency regime above 500 Hz comes from the photon shot originated from the phase fluctuation of the laser beam. This noise affects the readout of interference fringes at the dark port of the interferometer where the GW signal is detected. Several techniques can be applied to reduce the shot noise. HF-ET plans to use the squeezed states of the photons to optimize the sensitivity in certain frequency regimes below the standard quantum limit. As an additional remark, ET employs an ultra-high vacuum to reduce the surrounding gas pressure at 10^{-10} mbar [38]. The corresponding quality factor should be much higher than the mirror quality factor considered here. Therefore, the viscous damping due to the ambient gas collisions is insignificant [43].

Both internal thermal noise and photon shot noise are the dominant noises that potentially conceal the presence of our DM signals. In Fig. 1 we show the strain amplitude curve of ET which includes all the noise components [44]. The DM signals for two benchmark masses of 1 $\rm GeV/c^2$ and 50 $\rm PeV/c^2$, representing light and heavy DM, respectively, are also shown. The heights of the resonance peaks seem to be different in both cases. This is due to the difficulty in plotting very narrow peaks around the resonances. As one can see, the dark matter signal of heavy DM lies above the ET sensitivity curve at resonant frequencies, while the light DM signal is buried under the noises.

IV. SIGNAL-TO-NOISE RATIO

In this section we would like to analyze the detectability of the DM signal discussed previously in terms of the signal-to-noise ratio (SNR), ϱ^2. Basically, this is done by integrating the ratio of the DM signal over the noise in the corresponding frequency domain. Furthermore, one applies the appropriate filter to improve the SNR, which is optimally given by [45]

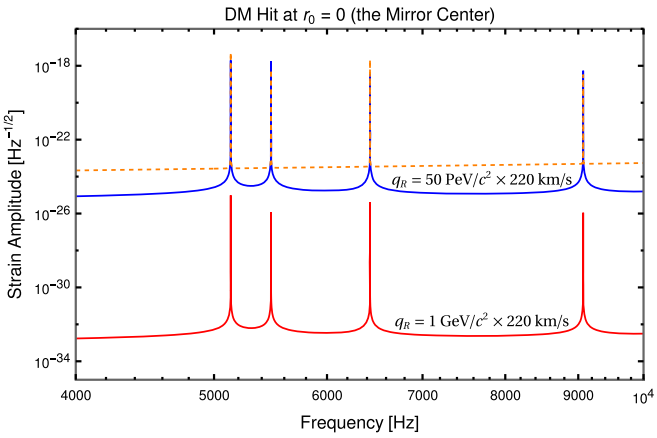

FIG. 1. Strain sensitivity of ET [44] (orange dashed line) and the hypothetical DM signals for light DM with a mass of 1 $\rm GeV/c^2$ (red line) as well as heavy DM with a mass of 50 $\rm PeV/c^2$ (blue line). The velocity of the dark matter particle is taken to be 220 km/s.

$$\varrho^2 \equiv \int_{f_{\min}}^{f_{\max}} \frac{\mathrm{d}f}{f} \frac{S_s(f)}{S_n(f)}, \tag{4.1}$$

where $S_s(f) = \tilde{h}_s^2(f)$ and $S_n(f) = \tilde{h}_n^2(f)$ are the PSD of the signal and the noise, respectively. Here, the integral runs over the frequency range probed by the corresponding detector. In our case, the SNR reads

$$\varrho^2(r, \theta, r_0, \theta_0) = \int_{f_{\min}}^{f_{\max}} \frac{\mathrm{d}f}{f} \frac{\tilde{h}_{\mathrm{DM}}^2(r, \theta, r_0, \theta_0, f)}{\tilde{h}_n^2(f)}. \tag{4.2}$$

In the following, we take the axis-symmetric mode ($m = 0$) to evaluate the SNR in Eq. (4.2) as well as $r_0 = \theta_0 = 0$, which corresponds to a DM collision at the center of the mirror. Furthermore, since the laser is focused at the center of the mirror, we set $r = 0$. This setup corresponds to the maximal $|\tilde{z}_{\mathrm{Elas}}(r, \theta, r_0, \theta_0, f)|$, as can be seen from Table III. To get a better understanding about the quantities that optimize the SNR, we make a simplification first before evaluating the actual SNR. Let us consider under which circumstances the DM signal overcomes the internal thermal noise. Based on Fig. 1, it is instructive to evaluate the SNR around the DM signal peak. We see from Eq. (3.1) that the PSD has a Lorentzian form peaked at $f = f_{0n}$ (for $m = 0$) with the associated full width at half maximum (FWHM) given by

$$\begin{aligned} f_{\max}^2 &= f_{0n}^2(1 + \phi_{0n}), \\ f_{\min}^2 &= f_{0n}^2(1 - \phi_{0n}). \end{aligned} \tag{4.3}$$

After expanding $\tilde{h}_{\mathrm{DM}}(f)$ and $\tilde{h}_{\mathrm{th}}(f)$ around the resonance ($f \approx f_{0n}$) and setting $\phi_{0n} \approx \frac{1}{Q_M}$, the SNR becomes

$$\begin{aligned} \varrho_{\mathrm{th}}^2 &= \int_{f_{\min}}^{f_{\max}} \frac{\mathrm{d}f}{f} \frac{\tilde{h}_{\mathrm{DM}}^2(0,0,0,0,f)}{\tilde{h}_n^2(f)} \approx \int_{f_{\min}}^{f_{\max}} \frac{\mathrm{d}f}{f} \frac{\tilde{h}_{\mathrm{DM}}^2(0,0,0,0,f)}{\tilde{h}_{\mathrm{th}}^2(f)} = \int_{f_{\min}}^{f_{\max}} \mathrm{d}f \frac{|\tilde{z}_{\mathrm{Elas}}(0,0,0,0,f)|^2}{x_{\mathrm{th}}^2(f)} \\ &= \frac{\pi^2 a^4}{(2\pi)^3} \frac{q_R^2}{2M_T} \frac{W_{0n}^4(0,0)}{(\int_0^a W_{0n}^2(r) r \mathrm{d}r)^2} \frac{1}{k_B T} \int_{f_{\min}}^{f_{\max}} \mathrm{d}f \frac{f}{f_{0n}^2 \phi_{0n}} \\ &= \frac{a^4}{16\pi} \frac{E_R}{E_{\mathrm{th}}} \left[\frac{W_{0n}^2(0,0)}{\int_0^a W_{0n}^2(r) r \mathrm{d}r} \right]^2 \frac{f_{\max}^2 - f_{\min}^2}{2 f_{0n}^2 \phi_{0n}} = \frac{a^4}{\pi} \frac{E_R}{E_{\mathrm{th}}} \left[\frac{W_{0n}^2(0,0)}{4 \int_0^a W_{0n}^2(r) r \mathrm{d}r} \right]^2 \\ &\approx \frac{1}{\pi} \frac{E_R}{E_{\mathrm{th}}} \left[\frac{J_0^2(0)}{2(J_0^2(\Delta_1(\lambda_{0n})) + J_1^2(\Delta_1(\lambda_{0n})))} \right]^2, \end{aligned} \tag{4.4}$$

where we have defined the recoil energy $E_R \equiv q_R^2/(2M_T)$ and the thermal energy $E_{\mathrm{th}} \equiv k_B T/2$ for a single degree of freedom. To obtain the last line, we set $\delta_i^2 > 0$ and used the fact that the first term on the right-hand side of Eq. (2.16) dominates over the second term. The integration boundary is given by Eq. (4.3).

Apart from the normal mode function, the SNR is proportional to the ratio of the dark matter recoil energy (E_R) and thermal energy (E_{th}). Thus, to optimize the SNR in this case, one needs a lighter mirror and lower temperature. This is in qualitative agreement with the toy model considered in Ref. [6]. However, lowering the mass of the mirror will not be suitable for current GW detectors as it enhances the radiation pressure noise at low frequencies and further limits the sensitivity of the detector. Furthermore, reducing the temperature would significantly increase the loss angle ϕ_{mn} relevant for the thermal mirror noise [40]. The only option left is to have DM with a higher recoil momentum q_R.

We see from the second line of Eq. (4.4) that the SNR is proportional to $q_R^2 = 2M_T E_R$. The recoil energy can be used to parametrize the SNR in any GW detector. In HF-ET, we focus on the middle peak of Fig. 1 around 6431 Hz to compute the SNR. For the integration boundary, one can use the FWHM as before. However, this is not recommended since the frequency resolution of HF-ET is bigger than the FWHM. Thus, we choose the following integration boundary:

$$f_{\min} = 6426\ \mathrm{Hz} \quad \text{and} \quad f_{\max} = 6436\ \mathrm{Hz}. \tag{4.5}$$

The resulting SNR as a function of E_R is shown in Fig. 2. It is clear that, in order to achieve a considerable signal for detection (namely, SNR > 1), one needs a recoil energy higher than about 10^{-30} J. Note that in our numerical results we take the typical velocity about 220 km/s of dark matter particles as the Earth passes through the dark matter halo. In this case, HF-ET should be able to detect DM with a mass heavier than PeV/c^2, such as the super-heavy DM suggested in Refs. [27,46]. On the other hand, the kinetic energy of light dark matter boosted by unknown sources may reach the PeV regime as well [47–54]. As a result, the recoil energy E_R will be enhanced and makes the detectability of such dark matter particles in ET become feasible.

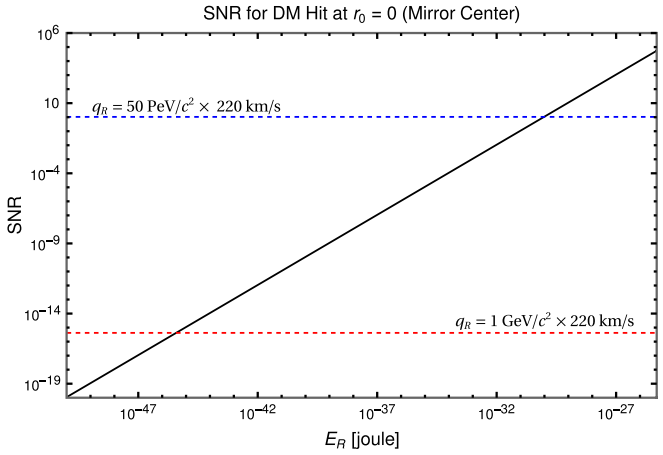

FIG. 2. SNR as a function of the recoil energy E_R (solid black line) for the Einstein Telescope. The corresponding SNRs for the light DM (red dashed line, $q_R = 1\ \mathrm{GeV/c^2} \times 220\ \mathrm{km/s}$, and $E_R = 3.85 \times 10^{-46}$ joule) and heavy DM (blue dashed line, $q_R = 50\ \mathrm{PeV/c^2} \times 220\ \mathrm{km/s}$, and $E_R = 9.61 \times 10^{-31}$ joule) are 4.20×10^{-16} and 1.05, respectively.

V. SUMMARY AND CONCLUSIONS

We described the scattering of DM particles and GW detectors, focusing on the HF-ET. We showed that DM induces elastic oscillations in the mirror employed in the interferometer arm of ET. This motion excites the resonance frequencies of the mirror and can be detected in the optomechanical setup used in ET.

Our work improved the previous calculations of the DM signal in two ways. First, by taking into account the thickness of the mirror, we found four resonance frequencies of the mirror inside the HF-ET detection band, as opposed to only a single resonance frequency found in the previous study. Furthermore, we demonstrated that the same resonance frequencies are excited by mirror thermal noise. This may conceal the hypothetical DM signal and hence cannot be neglected. To overcome the thermal noise, one needs to reduce both the mirror mass and its temperature.

We considered the detection of light DM and heavy DM with masses of 1 $\mathrm{GeV/c^2}$ and 50 $\mathrm{PeV/c^2}$, respectively, as our benchmarks. We found a linear relationship between the recoil energy induced by DM collisions and the SNR. The signal from heavy DM with a mass of the order of a few PeV could reach SNR $\gtrsim 1$, while the light DM would be buried by the thermal noise unless it is highly boosted.

ACKNOWLEDGMENTS

We would like to acknowledge the support of the National Center for Theoretical Sciences (NCTS). This work was supported in part by the Ministry of Science and Technology (MOST) of Taiwan under Grants No. MOST 109-2112-M-003-004-, 110-2112-M-003-003-, and 110-2811-M-003-505-.

[1] E. Aprile *et al.* (XENON Collaboration), Phys. Rev. D **102**, 072004 (2020).
[2] O. Adriani *et al.* (PAMELA Collaboration), Nature (London) **458**, 607 (2009).
[3] L. Accardo *et al.* (AMS Collaboration), Phys. Rev. Lett. **113**, 121101 (2014).
[4] B. P. Abbott *et al.* (LIGO Scientific and Virgo Collaborations), Phys. Rev. Lett. **116**, 061102 (2016).
[5] S. Tsuchida, N. Kanda, Y. Itoh, and M. Mori, Phys. Rev. D **101**, 023005 (2020).
[6] C. H. Lee, C. S. Nugroho, and M. Spinrath, Eur. Phys. J. C **80**, 1125 (2020).
[7] N. Seto and A. Cooray, Phys. Rev. D **70**, 063512 (2004).
[8] A. W. Adams and J. S. Bloom, arXiv:astro-ph/0405266.
[9] C. J. Riedel, Phys. Rev. D **88**, 116005 (2013).
[10] Y. V. Stadnik and V. V. Flambaum, Phys. Rev. Lett. **114**, 161301 (2015).
[11] A. Arvanitaki, S. Dimopoulos, and K. Van Tilburg, Phys. Rev. Lett. **116**, 031102 (2016).
[12] Y. V. Stadnik and V. V. Flambaum, Phys. Rev. A **93**, 063630 (2016).
[13] S. Dimopoulos, P. W. Graham, J. M. Hogan, M. A. Kasevich, and S. Rajendran, Phys. Rev. D **78**, 122002 (2008).
[14] P. W. Graham *et al.* (MAGIS Collaboration), arXiv:1711.02225.
[15] J. Coleman (MAGIS-100 Collaboration), Proc. Sci. ICHEP2018 (**2019**) 021 [arXiv:1812.00482].
[16] T. Cheng, R. Primulando, and M. Spinrath, Eur. Phys. J. C **80**, 519 (2020).
[17] L. Badurina *et al.* (AION Collaboration), J. Cosmol. Astropart. Phys. 05 (2020) 011.
[18] Y. A. El-Neaj *et al.* (AEDGE Collaboration), Eur. Phys. J. Quantum Technol. **7**, 6 (2020).
[19] B. Canuel *et al.* (MIGA Collaboration), Sci. Rep. **8**, 14064 (2018).
[20] B. Canuel *et al.* (ELGAR Collaboration), Classical Quantum Gravity **37**, 225017 (2020).
[21] M. S. Zhan *et al.* (ZAIGA Collaboration), Int. J. Mod. Phys. D **29**, 1940005 (2020).
[22] S. Dimopoulos, P. W. Graham, J. M. Hogan, and M. A. Kasevich, Phys. Rev. D **78**, 042003 (2008).
[23] P. W. Graham, J. M. Hogan, M. A. Kasevich, and S. Rajendran, Phys. Rev. Lett. **110**, 171102 (2013).

[24] P. W. Graham, J. M. Hogan, M. A. Kasevich, and S. Rajendran, Phys. Rev. D **94**, 104022 (2016).
[25] A. Branca *et al.*, Phys. Rev. Lett. **118**, 021302 (2017).
[26] C. J. Riedel and I. Yavin, Phys. Rev. D **96**, 023007 (2017).
[27] E. D. Hall, R. X. Adhikari, V. V. Frolov, H. Mller, and M. Pospelov, Phys. Rev. D **98**, 083019 (2018).
[28] S. Jung and C. S. Shin, Phys. Rev. Lett. **122**, 041103 (2019).
[29] A. Pierce, K. Riles, and Y. Zhao, Phys. Rev. Lett. **121**, 061102 (2018).
[30] S. Morisaki and T. Suyama, Phys. Rev. D **100**, 123512 (2019).
[31] H. Grote and Y. V. Stadnik, Phys. Rev. Research **1**, 033187 (2019).
[32] A. Kawasaki, Phys. Rev. D **99**, 023005 (2019).
[33] F. Monteiro, G. Afek, D. Carney, G. Krnjaic, J. Wang, and D. C. Moore, Phys. Rev. Lett. **125**, 181102 (2020).
[34] R. D. Mindlin and H. Deresiewicz, J. Appl. Phys. **25**, 1329 (1954).
[35] P. H. Wen, M. Adetoro, and Y. Xu, Eng. Anal. Boundary Elem. **32**, 870 (2008).
[36] A. W. Leissa, *Vibration of Plates*, Scientific and Technical Information Division (National Aeronautics and Space Administration, Washington, 1969), Vol. 160.
[37] S. Chakraverty, *Vibration of Plates* (CRC Press, Boca Raton, 2008).
[38] T. Irie, G. Yamada, and S. Aomura, J. Appl. Mech. **47**, 652 (1980).
[39] Y. Xiang and L. Zhang, J. Sound Vibr. **280**, 633 (2005).
[40] The Einstein Telescope Science Team, ET design study document, ET-0106C-10 [Online]. Available: etdsdocument, http://www.et-gw.eu/.
[41] M. Evans, S. Gras, P. Fritschel, J. Miller, L. Barsotti, D. Martynov, A. Brooks, D. Coyne, R. Abbott, and R. Adhikari *et al.*, Phys. Rev. Lett. **114**, 161102 (2015).
[42] S. Biscans, S. Gras, C. D. Blair, J. Driggers, M. Evans, P. Fritschel, T. Hardwick, and G. Mansell, Phys. Rev. D **100**, 122003 (2019).
[43] P. R. Saulson, Phys. Rev. D **42**, 2437 (1990).
[44] LIGO Document No. LIGO DCC T1500293-v13, https://dcc.ligo.org/LIGO-T1500293/public, accessed on August 20th, 2021.
[45] C. J. Moore, R. H. Cole, and C. P. L. Berry, Classical Quantum Gravity **32**, 015014 (2015).
[46] M. Ahmadvand, J. High Energy Phys. 10 (2021) 109.
[47] Y. Ema, F. Sala, and R. Sato, Phys. Rev. Lett. **122**, 181802 (2019).
[48] C. V. Cappiello and J. F. Beacom, Phys. Rev. D **100**, 103011 (2019); **104**, 069901(E) (2021).
[49] W. Yin, Eur. Phys. J. Web Conf. **208**, 04003 (2019).
[50] G. Guo, Y. L. S. Tsai, and M. R. Wu, J. Cosmol. Astropart. Phys. 10 (2020) 049.
[51] C. Xia, Y. H. Xu, and Y. F. Zhou, J. Cosmol. Astropart. Phys. 02 (2022) 028.
[52] G. Guo, Y. L. S. Tsai, M. R. Wu, and Q. Yuan, Phys. Rev. D **102**, 103004 (2020).
[53] J. C. Feng, X. W. Kang, C. T. Lu, Y. L. S. Tsai, and F. S. Zhang, arXiv:2110.08863.
[54] T. Bringmann and M. Pospelov, Phys. Rev. Lett. **122**, 171801 (2019).